sustainability

MDPI

Article

Investigating Asphaltene Precipitation and Deposition in Ultra-Low Permeability Reservoirs during CO_2-Enhanced Oil Recovery

Dandan Yin, Qiuzi Li and Dongfeng Zhao *

College of Petrochemical Engineering & Environment, Zhejiang Ocean University, Zhoushan 316021, China; yindandan@zjou.edu.cn (D.Y.); 18868006623@163.com (Q.L.)
* Correspondence: aayindan@163.com.com

Abstract: CO_2 flooding is an economically feasible and preferred carbon capture, storage, and utilization technology. Asphaltene deposition is a common problem in the process of CO_2 injection because it may cause reservoir damage. The mechanism of asphaltene precipitation damage to the formation remains elusive. Experiments were conducted to reveal the pore-scale formation damage mechanism in ultra-low permeability reservoirs caused by asphaltene precipitation during CO_2 flooding. Initially, the precipitation onset point for asphaltene within the crude oil-CO_2 system was determined using a high-pressure tank equipped with visual capabilities. Subsequently, CO_2 flooding experiments were conducted on ultra-low permeability cores under miscible and immiscible conditions, with the support of nuclear magnetic resonance (NMR) to quantitatively evaluate the impact of asphaltene precipitation on ultra-low permeability reservoirs. The results indicate that within the pressure range from the asphaltene precipitation onset point to the minimum miscibility pressure (MMP). The level of asphaltene precipitation rises as CO_2 injection pressure increases. In the miscible flooding stage, asphaltene precipitation can still occur, but to a lesser extent. Notably, asphaltene deposition predominantly occurs in larger pores; above the MMP, the permeability decreases significantly as asphalt particles agglomerate, resulting in notable pore-throat blockages. While asphaltene deposition has a minimal impact on porosity, the bridging effect of asphaltene particles reduces permeability.

Keywords: CO_2 flooding; asphaltene precipitation; formation damage; ultra-low permeability reservoir

Citation: Yin, D.; Li, Q.; Zhao, D. Investigating Asphaltene Precipitation and Deposition in Ultra-Low Permeability Reservoirs during CO_2-Enhanced Oil Recovery. *Sustainability* **2024**, *16*, 4303. https://doi.org/10.3390/su16104303

Academic Editor: Francesco Ferella

Received: 14 March 2024
Revised: 8 May 2024
Accepted: 15 May 2024
Published: 20 May 2024

1. Introduction

Total energy-related CO_2 emissions increased by 1.1% and reached 37.4 billion tons in 2023 [1]. Carbon capture, storage, and utilization (CCSU) emerges as a pivotal strategy in the fight against climate change [2]. CO_2 flooding stands out for its dual benefits: it can significantly cut down greenhouse gas emissions—given that approximately 50% to 60% of the injected CO_2 remains sequestered underground permanently—and it can also enhance oil recovery. This enhancement is achieved by reducing the viscosity of crude oil and the oil-gas interfacial tension, thereby expanding the volume of crude oil and initiating a process known as dissolved gas flooding [3–7]. In a light oil reservoir, 50 to 60% of the original oil-in-place (OOIP) remains after primary recovery [8]. About 38% of the world's reservoirs and about 46% of reservoirs in China are ultra-low permeability reservoirs [9]. These reservoirs are characterized by their minuscule pores and fine throats, which result in an unusually large specific surface area, making them particularly susceptible to contamination and damage [10–12]. The protection of these reservoirs is of paramount importance [13,14]. The interaction between reservoir oil and CO_2 is crucial to achieving multi-contact miscibility. When CO_2 is sufficiently dissolved in the oil, it can trigger asphaltene precipitation, which markedly alters the physicochemical properties of the oil [15–17]. Asphaltenes, insoluble in lower normal alkanes but soluble in benzene and

toluene, are colloidal particles within crude oil [18–20]. They are composed of molecular clusters surrounded by resins, forming micelles that increase their solubility [21]. During CO_2 flooding, the interaction between crude oil and CO_2 leads to the occupation of CO_2 molecules in the interfacial region of these asphaltene clusters. This results in a decrease in resin concentration, potentially leading to the inability to form micelles and the subsequent aggregation and precipitation of asphaltene molecules [22–24]. As injection pressure increases, more CO_2 dissolves in the crude oil, further reducing the concentration of resins that act as stabilizers for asphaltenes. This makes the asphaltene clusters more prone to flocculation and precipitation [25]. Asphaltene deposition is a common issue during CO_2 injection, and the associated formation damage typically manifests in four ways: (I) reduction in permeability or physical blockage, (II) alteration of wettability, (III) decrease in oil viscosity, and (IV) the formation of emulsions [26]. Among these, mechanism (I) is identified as the primary cause of formation damage [27,28]. The deposition process begins with the adsorption of asphaltenes onto the rock surface, followed by hydrodynamic retention or capture of particles at the pore throat, leading to diminished oil mobility. Changes in pressure, temperature, and petroleum composition can further affect the surface properties and rheology of crude oil [29]. The occurrence of sedimentation poses significant challenges to both upstream and downstream operations [30–38]. Even in low-permeability reservoirs with low asphaltene content, such as the Hassi Messaoud field, which had an asphaltene content of just 0.062%, deposition problems have been reported from the onset of production [39]. However, the detailed effects of asphaltene deposition on pore sizes under various injection conditions have not been extensively explored in previous research.

Current research on the impact of asphaltene deposition on recovery is primarily focused on analyzing the extent of recovery reduction, with the underlying microscopic mechanisms remaining unclear. This study aims to investigate the initial precipitation of asphaltenes from crude oil and the intricate patterns of asphaltene deposition above the onset point. It also seeks to determine the precipitation onset point for asphaltenes in a light crude oil-CO_2 system. CO_2 flooding experiments are conducted to elucidate the mechanisms of physical damage to ultra-low permeability reservoirs during the flooding process.

2. Materials and Methods

2.1. Materials

The composition of the Triassic-produced water from Block X within the Ordos Basin was analyzed. The purity of CO_2 used in the experiment is 99.99%. Simulated formation water is prepared, and the scale-forming ions (Ba^{2+}, Sr^{2+}, Ca^{2+}, Mg^{2+}) in the formation water are replaced with K^+ and Na^+. The resulting Total Dissolved Solids (TDS) concentration was measured at 92,455 mg/L.

The natural core samples were extracted from the Triassic X reservoir located in Block X of the Ordos Basin. After a thorough cleaning and drying process, the cores were subjected to a 48 h vacuum treatment. Subsequently, they were saturated with the simulated formation water to ascertain their porosity. The core permeability was then measured by conducting a formation water injection test. The measured porosity values varied from 10.38% to 13.73%, while the absolute permeability values ranged from 0.33 to 0.38×10^{-3} μm^2, as shown in Table 1.

Table 1. Basic Parameters of the Core Samples.

Core NO.	Length, cm	Pore Volume, mL	Porosity,%	K, 10^{-3} μm^2
1	7.62	3.88	10.38	0.35
2	7.62	3.93	10.51	0.34
3	6.86	4.62	13.73	0.38
4	6.78	3.53	10.61	0.33

Crude oil is from the Changqing Oilfield. The components of live oil tested by high-temperature gas chromatography (HTGC) are shown in Table 2.

Table 2. The components of crude oil.

Component	W, %	Component	W, %	Component	W, %	Component	W, %
N_2	1.52	C_7	3.84	C_{17}	1.98	C_{27}	1.08
CO_2	0.01	C_8	6.1	C_{18}	1.69	C_{28}	1.06
C_1	24.58	C_9	4.68	C_{19}	1.6	C_{29}	1.01
C_2	4.37	C_{10}	3.84	C_{20}	1.37	C_{30}	0.85
C_3	3.16	C_{11}	3.37	C_{21}	1.23	C_{31}	0.65
iC_4	1.21	C_{12}	3.08	C_{22}	1.21	C_{32}	0.52
nC_4	0.86	C_{13}	2.85	C_{23}	1.1	C_{33}	0.45
iC_5	0.72	C_{14}	2.77	C_{24}	1.01	C_{34}	0.4
nC_5	0.97	C_{15}	2.25	C_{25}	0.98	C_{35}	0.37
C_6	1.52	C_{16}	2.16	C_{26}	1.02	$C_{36}+$	6.29

The properties of crude oil were tested with Pressure-Volume-Temperature (PVT). The bubble point pressure was 7.8 MPa. Furthermore, the Minimum Miscibility Pressure (MMP) of the crude oil, ascertained through the slim tube displacement experiment, was established at 16.0 MPa. According to the ASTMD2007-03 standard [40], the mass fraction of the crude oil's n-heptane-insoluble asphaltenes was measured to characterize the oil's colloidal stability. A comprehensive SARA (Saturates, Aromatics, Resins, and Asphaltenes) analysis, delineating the complex composition of the crude oil, is presented in Table 3 for an in-depth understanding of its chemical constituents.

Table 3. SARA of crude oil.

Component	Asphaltenes	Resins	Aromatics	Saturates	Total Yield
W, %	1.32	8.59	13.52	63.78	87.21

2.2. Experimental Equipment

The High-Temperature High-Pressure (HTHP) Visible Reaction Apparatus: As depicted in Figure 1, the HTHP visible reaction vessel is designed for observing chemical processes under extreme conditions. It features an internal volume capacity of 2000 mL and is engineered to withstand a maximum pressure of 30 MPa. The pressure within the vessel is regulated by an ISCO pump, allowing for the observation of solution changes through a sapphire observation window. Within the vessel, a heating mechanism is integrated, offering a temperature range from 20 to 180 degrees Celsius. To ensure optimal illumination for the CO_2-saturated oil layer, a cold light source and a frosted glass sheet are strategically positioned beneath the reactor. A microscope is mounted atop the apparatus, enabling the observation of the evolving layer patterns within the light crude oil-CO_2 system within the vessel. For the precise capture of these visual changes, a high-resolution CCD camera, equipped with 6 million pixels, is affixed to the microscope. The geometric dimensions of the asphaltene aggregates are subsequently determined by analyzing the captured images using Sigma Scan Pro 5 software. The internal pressure of the reactor is controlled by the injection of CO_2 into the ISCO pump, while the temperature is maintained with the aid of a high-precision heating device.

Figure 2 illustrates the schematic diagram of the high-pressure core-flooding apparatus, which is specifically designed for conducting CO_2 flooding experiments. The setup includes two separate high-pressure cylinders that contain simulated formation water—free of scale-forming ions—and CO_2, respectively. A dual ISCO syringe pump is employed to inject fluids from these high-pressure cylinders into the core holder, which is capable of withstanding a maximum pressure (Pmax) of 80 MPa and a maximum temperature (Tmax) of 100 °C. An additional pump is dedicated to maintaining the confining pressure within the system. In conjunction with this, another pump and a back-pressure valve are strategically utilized to finely regulate and maintain the back pressure throughout the experimental process. To ensure uniform temperature control, both the high-pressure cylinders and the core holder are securely positioned within a constant-temperature oven.

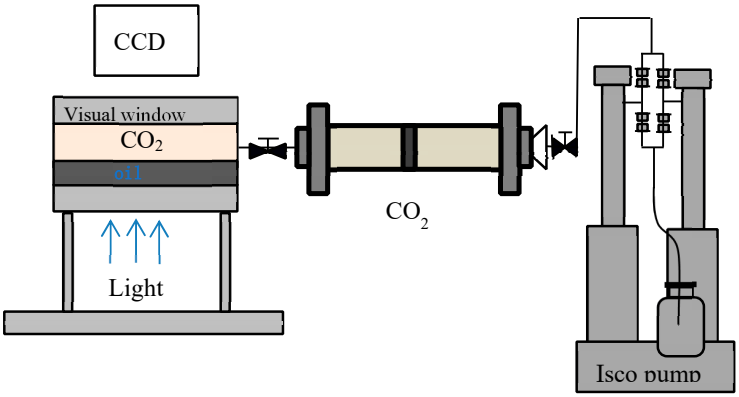

Figure 1. HTHP visual reaction system.

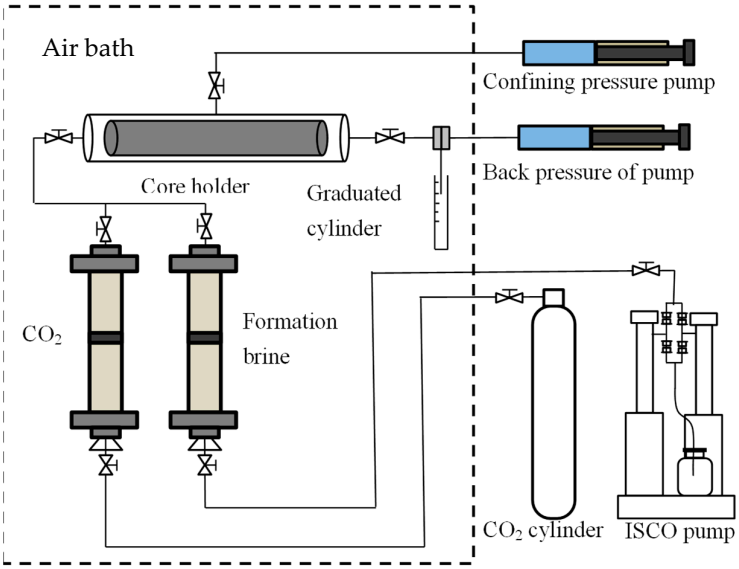

Figure 2. Schematic diagram of the core-flooding set-up.

2.3. Experimental Methods and Procedures

The Measurement of precipitation onset point for asphaltenes. A multitude of techniques have been established for identifying the onset point of asphaltene precipitation. These methods encompass a range of analytical approaches, such as monitoring electrical conductivity, assessing crude oil viscosity, measuring interfacial tension, conducting gravimetric analysis, evaluating light transmission, and employing visualization techniques [34,41–44]. In this study, we have opted to utilize a visualization apparatus to ascertain the specific pressure threshold at which asphaltene precipitation initiates within the crude oil-CO_2 system. Figure 2 presents a schematic representation of the experimental setup designed to determine the asphaltene precipitation onset point within a light crude oil layer saturated with CO_2. The relative deposition of asphaltenes was quantified by observing changes in the visual imagery under varying pressure conditions. The images captured during the experiment were subsequently analyzed using Sigma Scan Pro 5 software to measure the relative deposition levels. The critical pressure value, at which a marked increase in the relative deposition of asphaltenes was observed, was calculated employing Equation (1). This calculated pressure signifies the onset point for asphaltene precipitation.

$$\delta = \frac{S_A}{S_O} \times 100\% \quad (1)$$

where δ is the relative deposition of asphaltenes, S_A is the area of asphaltene deposited, and S_O is the area of the visual window.

Core-flooding experiment. All core samples underwent a 24 h vacuum treatment to ensure complete saturation with simulated formation water. Each core was subsequently subjected to Nuclear Magnetic Resonance (NMR) analysis using a SPEC-023-B device. This process recorded the transverse relaxation time (T_2) of hydrogen nuclei within the brine in the core, along with the signal amplitude. Given that the T_2 value and its corresponding signal amplitude are indicative of the size and volume of the pore spaces housing the hydrogen nuclei, the T_2 spectrum can be translated into a distribution of the core's pore radii. Post-NMR saturation with brine, the core was infused with oil, facilitating the calculation of the initial oil saturation (Soi) and the irreducible water saturation (Swc) for each core. This continued until no water was produced. The core holder was then exposed to a pressurized and heated environment for a duration of 12 h, after which CO_2 was introduced at a controlled rate of 0.1 mL/min. Back pressures of 8, 13, 16, and 20 MPa were sequentially applied, with CO_2 injection ceasing upon the cessation of oil production. Throughout the process, the injection and production pressures, along with the volumes of injected and produced fluids, were continuously monitored, recorded, and logged automatically by a computer system. The produced fluids, encompassing brine, oil, and gas, were systematically collected and quantified using a gas-liquid cyclone separator and a mass flow meter.

The SARA (Saturates, Aromatics, Resins, and Asphaltenes) analysis was conducted on the produced oil. Since the simulated formation water was devoid of scale-forming ions, the impact of inorganic precipitation was effectively eliminated. The experimental displacement timeframe was significantly shorter than the CO_2-rock-water interaction timeframe reported in other studies [45,46], allowing us to disregard the influence of formation water reactions on core porosity. Following CO_2 flooding, kerosene was injected into the core to displace any remaining fluids. Subsequently, n-heptane was utilized to remove the kerosene, ensuring that the asphaltene deposits within the core's pores and throats were preserved. The core was then dried and analyzed to measure changes in permeability and porosity attributable to the asphaltene deposits. The core was saturated with simulated formation water, and the distribution of pore throats of varying sizes was reassessed using NMR. The porosity loss rate (η_ϕ), representing the extent of porosity reduction post-CO_2 flooding, was calculated using the formula presented in Equation (2). The permeability change rate was determined by Equation (3).

$$\eta_\varphi = \frac{\varphi_A - \varphi_{A0}}{\varphi_{A0}} * 100\% \quad (2)$$

where η_φ is the porosity change rate, φ_{A0} is the porosity before the CO_2 flooding, and φ_A is the porosity of the core after CO_2 flooding and oil washing with n-heptane.

$$R = \frac{K_d - K_0}{K_0} * 100\% \quad (3)$$

where R is the permeability change rate, K_d is the permeability before the CO_2 flooding, and K_o is the permeability of the core after CO_2 flooding and oil washing with n-heptane.

3. Results and Discussion

3.1. The Precipitation Onset Point for Asphaltenes

The solubility of asphaltenes in crude oil is influenced by a combination of temperature, pressure, and the specific composition of the oil. In a reservoir at a constant depth, the temperature can be considered relatively stable over time. The reactor was pressurized to 8 MPa with CO_2, after which the prepared live oil was introduced into the system. The pressure within the reactor was incrementally increased by 0.2 MPa per step, starting from 8 MPa, while conducting the real-time monitoring of visual changes. To attain equilibrium within the system, the solution was permitted to deposit asphaltenes onto a substrate for approximately two hours. The substrate was observed laterally through a microscope, which captured a series of continuous static images of the glass surface. Equilibrium was

deemed to have been reached when no further deposition of asphaltenes was observed on the substrate, a condition that was continuously verified by the monitoring cell. Initially, minimal changes in the visual imagery were noted in response to pressure alterations. There was no significant asphaltene deposition observed upon the initial contact of CO_2 with crude oil, resulting in a clear and transparent appearance, as depicted in Figure 3a. Upon elevating the experimental pressure to 10 MPa, a sparse distribution of small dots became visible on the imagery, as showcased in Figure 3b. The relative deposition, quantified at 3.12%, was ascertained through analysis using Sigma Scan Pro 5 software. When the experimental pressure was elevated to 12.6 MPa, a pronounced shift was observed as the image grew noticeably darker, as illustrated in Figure 3c. This indicated that a localized area of asphaltene had precipitated onto the window under these pressure conditions. The image was now populated with numerous small dots, and the relative deposit had risen to 35.06%. As the pressure within the reactor continued to escalate, the asphaltene particles visible in the images became progressively larger and more opaque, signaling an accelerated rate of asphaltene precipitation. A substantial deposition of asphaltenes is evident in Figure 3d–f, highlighting the impact of increasing pressure on asphaltene solubility and deposition.

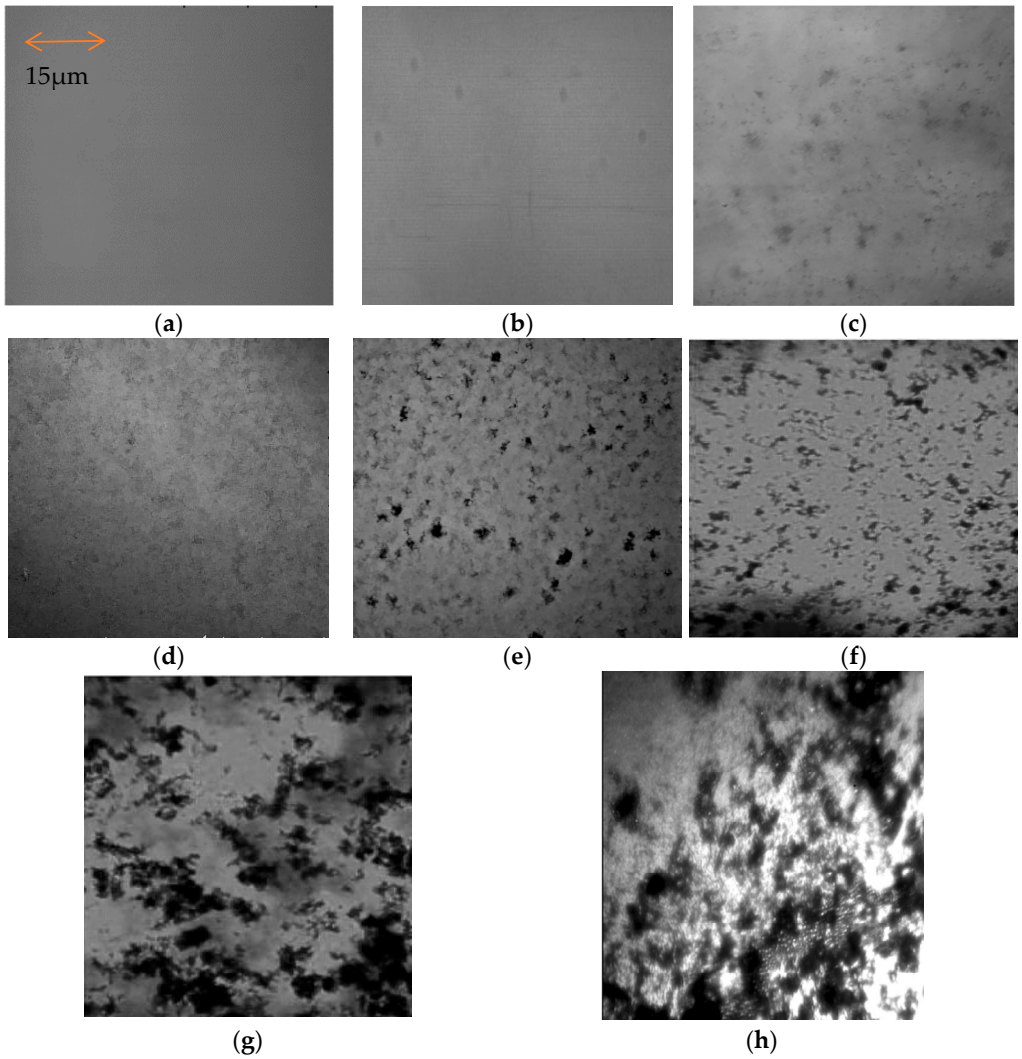

Figure 3. Asphaltene precipitation image at different pressures: (**a**) 8 MPa; (**b**) 10 MPa; (**c**) 12.6 MPa; (**d**) 13.4 MPa; (**e**) 14.6 MPa; (**f**) 15.2 MPa; (**g**) 16 MPa, and (**h**) 20 MPa.

When the pressure is elevated to 16 MPa, there is a notable aggregation of asphaltene particles, leading to their flocculation. Concurrently, CO_2 and crude oil may reach a state of

miscibility, as depicted in Figure 3g. This phenomenon can be attributed to the increasing solubility of CO_2 within the crude oil as the system pressure rises. Given their small size, CO_2 molecules progressively infiltrate the space ordinarily occupied by the stabilizing colloids that surround the asphaltene particles. This action compromises the stability of the asphaltene, causing the protective colloids to be continuously released into the crude oil, thereby triggering the precipitation of asphaltenes. At this juncture, the measured relative deposition stands at 62.12%. Upon further increasing the pressure to 20 MPa, as illustrated in Figure 3h, the asphaltene particles coalesce to form larger precipitates within the CO_2-saturated oil layer, manifesting as agglomerates. Referring to the relationship curve between the relative deposition amount and pressure, as presented in Figure 4, it becomes evident that there is a marked escalation in the relative deposition amount at a pressure of 12.6 MPa. Consequently, it can be deduced that at a temperature of 50 °C, the onset of asphaltene precipitation from CO_2-saturated oil occurs at a pressure threshold of 12.6 MPa, which is identified as the precipitation onset point for asphaltenes.

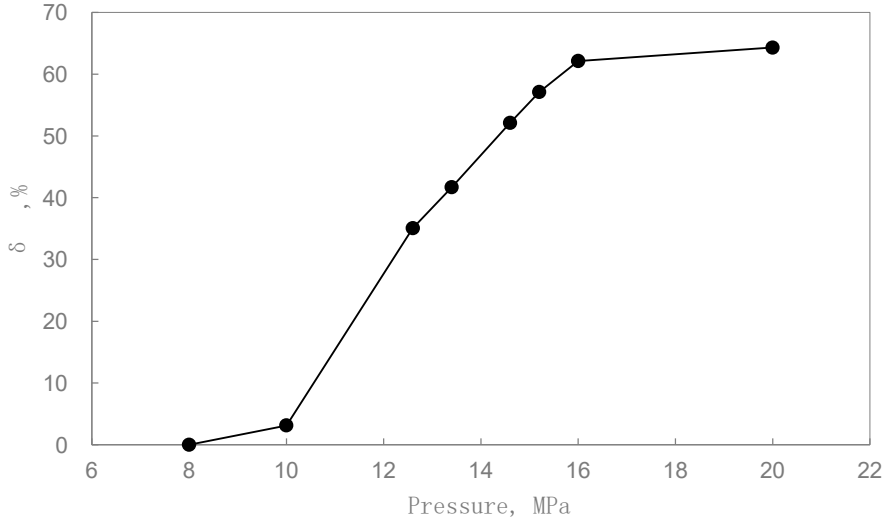

Figure 4. Relative deposition of asphaltenes versus pressures.

3.2. Effect of Asphaltene Precipitation on Formation Damage during CO_2 Flooding

CO_2 flooding efficiency. CO_2 flooding experiments were conducted at a constant temperature of 50 °C across a range of pressures. The CO_2 was introduced at a steady rate of 0.2 mL/min. The experimental parameters for the CO_2 flooding process are detailed in Tables 1 and 2. Given that the pressure at which asphaltene precipitation commences is identified as 12.6 MPa, and the Minimum Miscibility Pressure (MMP) is established at 16 MPa, the back-pressure for the core flooding experiments was accordingly set at 8 MPa, 13 MPa, 16.0 MPa, and 20 MPa. As illustrated in Figure 5, the recovery factor (RF) increases with an increasing pore volume (PV) of CO_2 injected. For each pressure setting, the RF attains its zenith upon the injection of 1 PV of CO_2. After the injection of 1.4 PV of CO_2, no further oil production was observed across the experiments. During the immiscible displacement phase, an increment in injection pressure leads to a proportional rise in the quantity of CO_2 dissolved within the crude oil, thus enhancing oil recovery rates. Upon surpassing the MMP, the rate of recovery increase diminishes, eventually plateauing as the system reaches its maximum recovery potential. The primary rationale behind this trend is the escalating dissolution of CO_2 into crude oil with rising pressure. Once the pressure surpasses 16 MPa, the RF attains its peak value, which is approximately 70%. Under miscible conditions, any subsequent rise in pressure results in only a marginal increase in RF, which ultimately stabilizes at a near-constant maximum value.

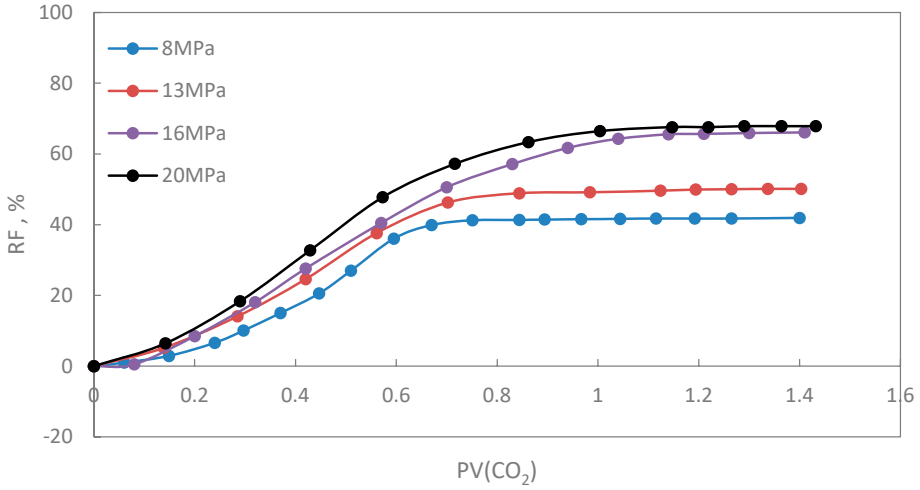

Figure 5. RF of CO_2 flooding versus PV of injected CO_2.

Additionally, Table 4 presents the asphaltene content of the oil produced during the experiments. The findings indicate that the asphaltene content in the produced oil is slightly lower than that in the crude oil when the pressure exceeds 8 MPa. The primary mechanisms at play during CO_2 flooding are the dissolution expansion and displacement effects, whereas the CO_2 extraction effect is considered to be insignificant. A significant reduction in asphaltene content within the produced oil is observed upon increasing the pressure from 13 MPa to 16 MPa. However, once the pressure surpasses the Minimum Miscibility Pressure (MMP), the variation in asphaltene content in the produced oil is minimal. This suggests that a greater amount of asphalt remains within the core during the immiscible flooding stage (P < 16 MPa), particularly at higher injection pressures. Conversely, the most substantial precipitation of asphaltene within the core occurs during the CO_2 miscible flooding phase (P > 16 MPa). In summary, as evidenced by Table 4, the asphaltene content in the oil produced during the CO_2 miscible flooding process is at its nadir. This implies that the injected CO_2 is capable of effectively displacing a substantial portion of the crude oil, thereby achieving the highest possible recovery factor (RF).

Table 4. SARA of the crude oil.

P, MPa / Content, %	8	13	16	20
Asphaltenes	1.22	0.83	0.14	0.11
Resins	8.59	7.79	7.62	6.42
Aromatics	13.52	13.44	12.58	12.55
Saturates	63.78	59.98	59.37	59.37
Total yield	87.11	82.04	79.71	78.45

Reduction in core permeability and porosity after CO_2 flooding. Post-displacement, the residual fluids within the core were purged using n-heptane, leaving behind the asphaltene precipitates within the pores and throats. A gas porosity and permeability testing apparatus was subsequently employed to measure the core's permeability and porosity after the drying process. Figure 6 demonstrates that following the flooding process, the core's gas permeability declines with an increase in CO_2 pressure. The reductions in both porosity and permeability are minimal (4% and 5%, respectively) for pressures below 13 MPa. However, the permeability experiences a more substantial decrease of over 18.67% at pressures exceeding 13 MPa, and it drops by approximately 50% when the pressures are above 16 MPa. As depicted in Figure 7, the core's porosity exhibits only a modest variation, ranging from a decrease of 2% to an increase of 7.7%. A slight increase in porosity is observed with the rise in pressure. By comparing the changes in porosity, it can be inferred that the core permeability underwent significant alterations during the flooding process.

Notably, there was an approximate 50% reduction in core permeability, accompanied by only a 7.7% variation in porosity. This discrepancy suggests the substantial impact of asphaltene deposition through adsorption and bridging effects, with the formation of bridge plugs likely playing a critical role. The ultra-low permeability core's porosity experienced only a slight change due to the more pronounced decrease in permeability, which was less influenced by the sedimentary adsorption effect. This reduction in permeability can be attributed to the obstruction of pore throats by the asphaltene deposits, highlighting the significance of pore throat blockage in the overall permeability reduction.

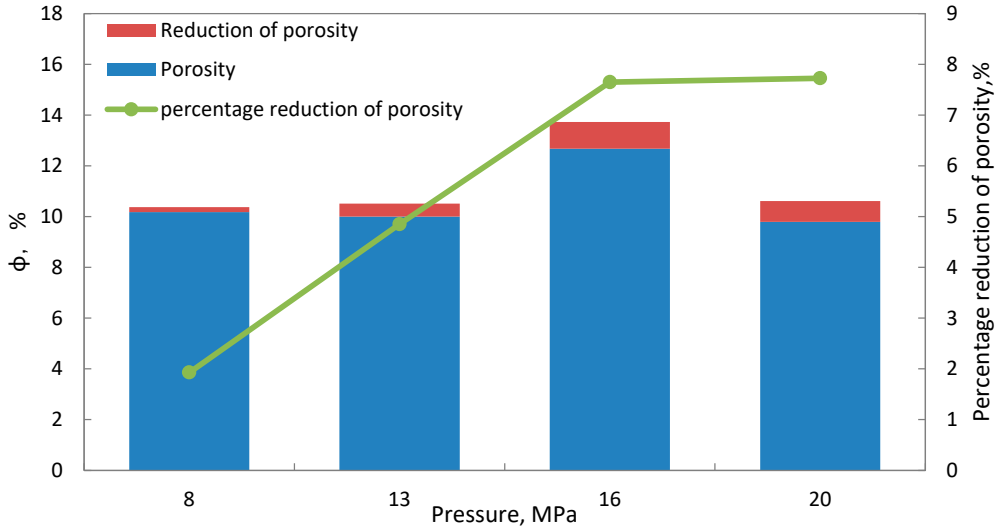

Figure 6. Permeability at different pressures before and after CO_2 flooding.

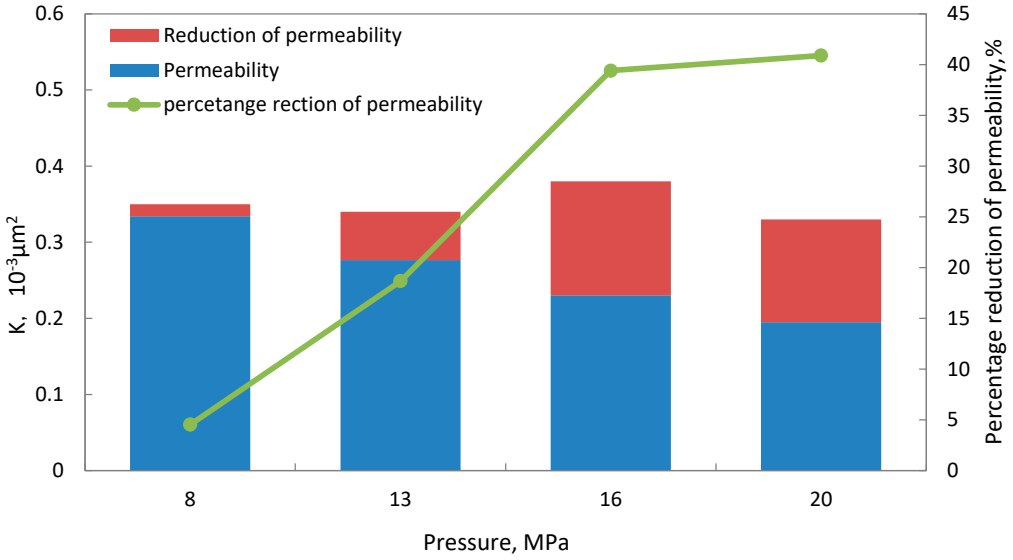

Figure 7. Core porosity under different pressures before and after CO_2 flooding.

Comparison of oil recovery in different-sized pores of CO_2 flooding. Four distinct core samples, each subjected to CO_2 flooding at back pressures of 8 MPa, 13 MPa, 16 MPa, and 20 MPa, were selected for subsequent Nuclear Magnetic Resonance (NMR) testing. Figure 8 presents a comparative analysis of the T_2 relaxation responses from these three core samples, both before and following the CO_2 flooding procedure. The T_2 response area is indicative of the relative oil content within the core, with larger areas signifying a higher concentration of oil. Distinct T_2 spectra of varying intensities were observed upon the conclusion of the CO_2 flooding experiments under each condition. Across all four pressure conditions, a more significant reduction in the right peak of the T_2 response was noted as

compared to the left peak. This observation suggests that crude oil within larger pores (ranging from 10 to 100 ms) and smaller pores (from 0.01 to 10 ms) is more susceptible to being displaced and subsequently recovered by CO_2. During the immiscible flooding stage, CO_2 predominantly displaces the crude oil residing in the larger pores, as evidenced in Figure 8a,b. In contrast, under miscible conditions, there is a substantial recovery of crude oil from the smaller pores as well, as depicted in Figure 8c,d. This indicates a more comprehensive extraction of oil from the core, facilitated by the miscibility of CO_2 with crude oil under higher pressure conditions.

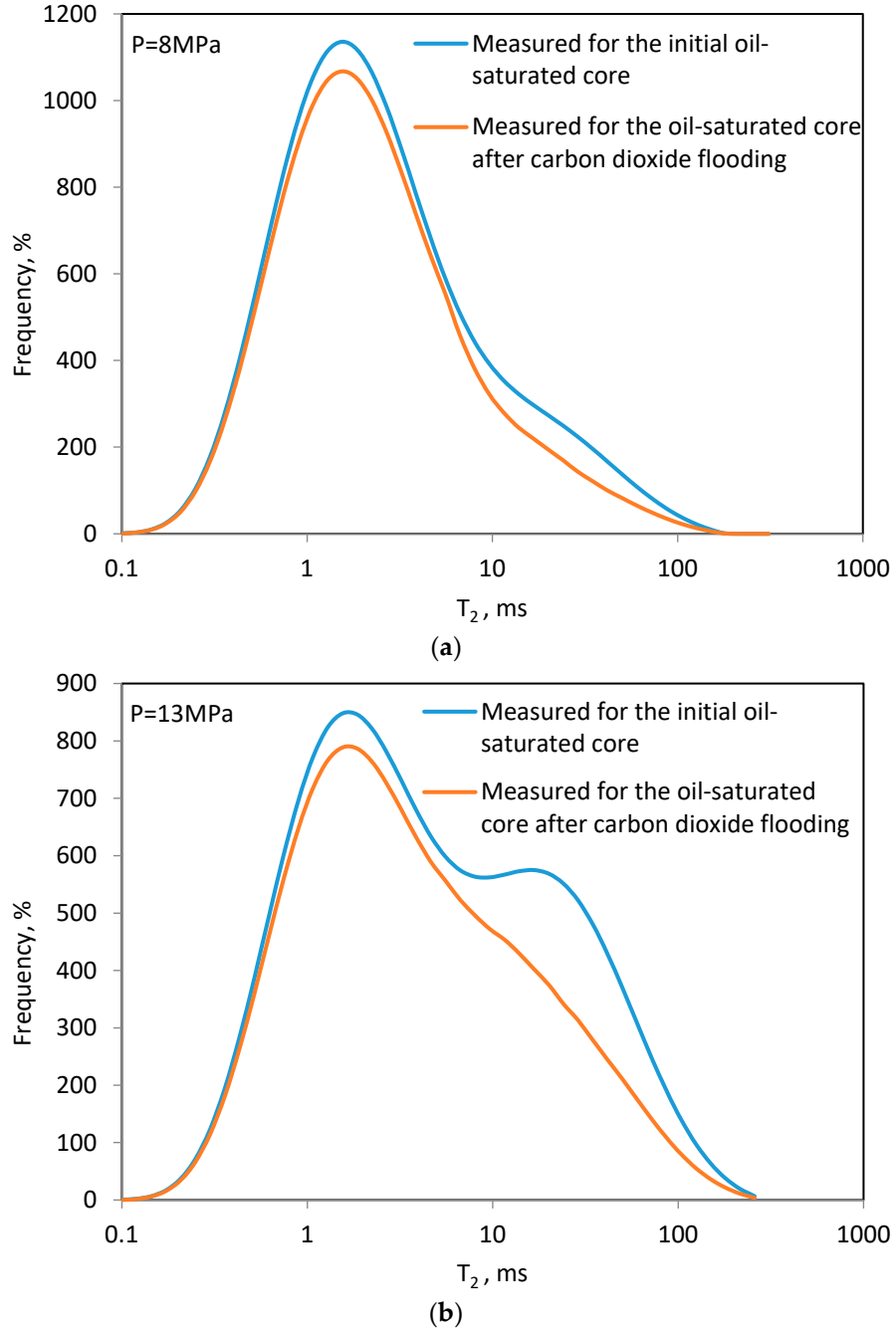

Figure 8. *Cont.*

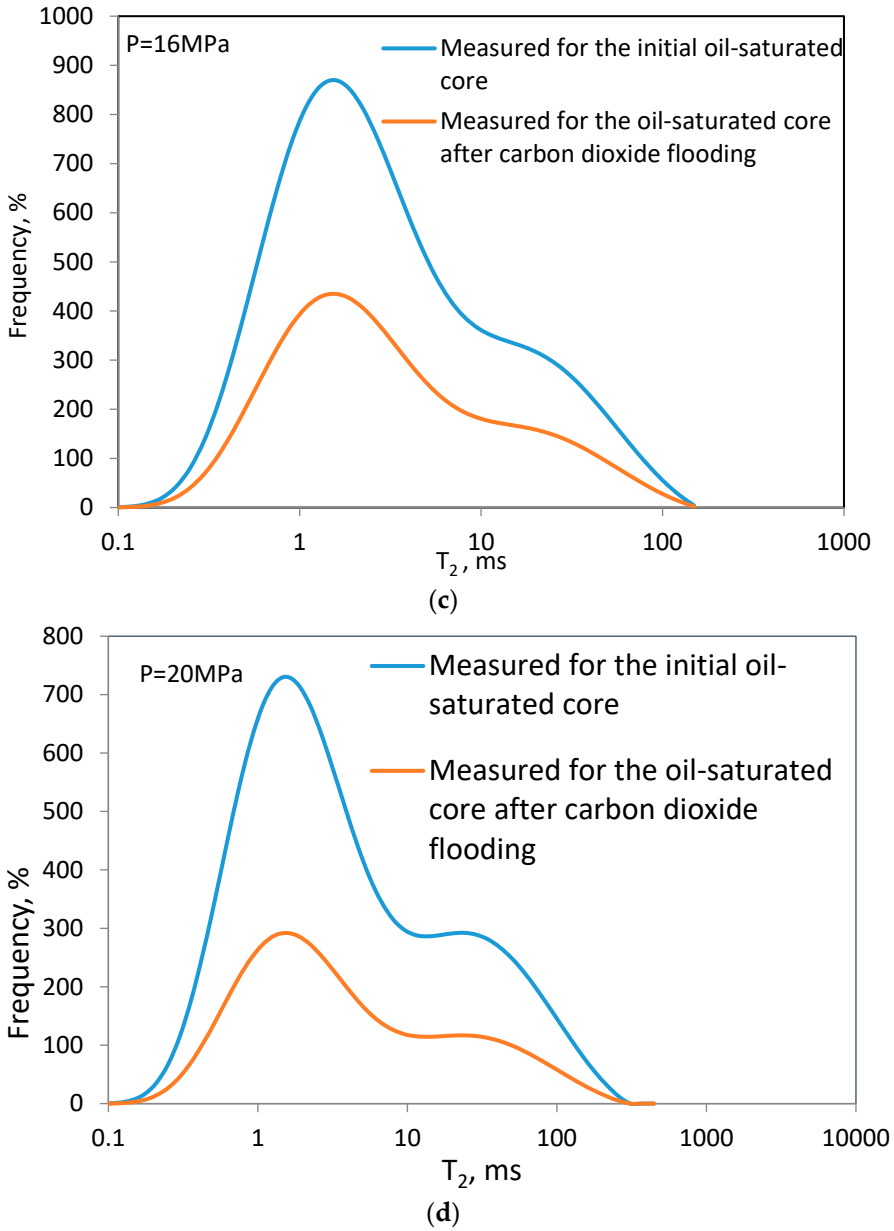

Figure 8. Comparison of T_2 response measured for the initial oil-saturated core and that measured for the oil-saturated core after CO_2 flooding conducted at (**a**) 8 MPa; (**b**) 13 MPa; (**c**) 16 MPa; and (**d**) 20 MPa.

Effect of Pore-Throat Microstructures on Formation Damage. The NMR spectra of the core samples, obtained at various pressures before and after CO_2 flooding, are presented in Figure 9. The primary peak in the T_2 spectrum, centered within the relaxation period of 0.5–10 ms, is indicative of the small pore and throat dimensions characteristic of the four cores employed in the study. Upon examination of the NMR data post-CO_2 flooding, it was observed that the overall alteration in the core's pore structure across the different pressures was not substantial. However, modifications within the larger pores were more pronounced and exhibited a discernible pattern. Specifically, an increase in pressure corresponded to a proportional decrease in the signal intensity from the larger pores, suggesting a direct relationship between pressure and the state of the larger pore spaces within the core.

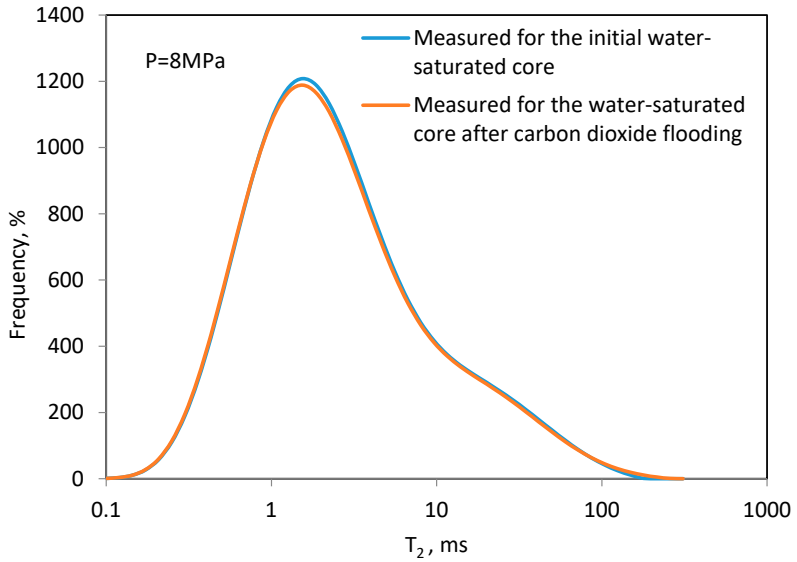

(**a**)

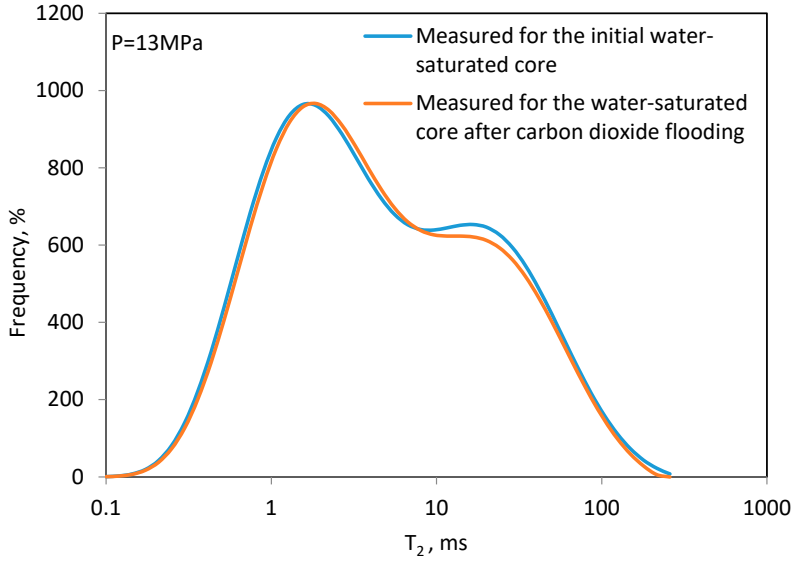

(**b**)

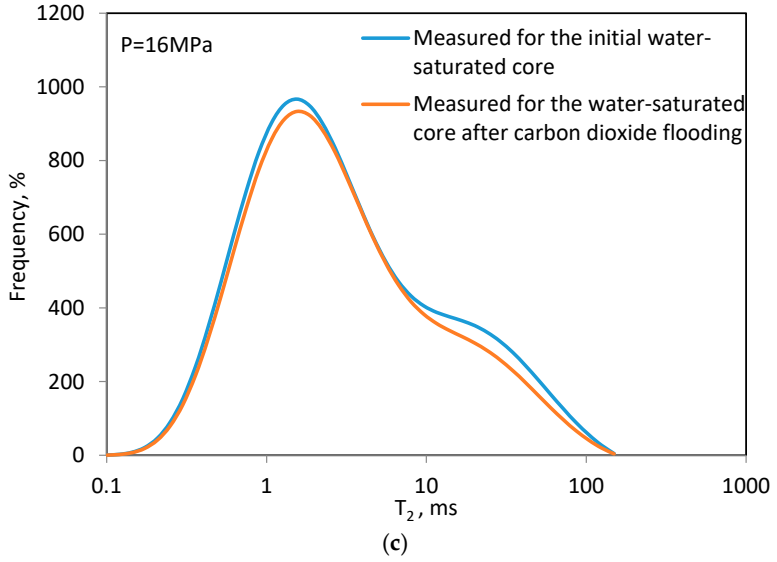

(**c**)

Figure 9. *Cont.*

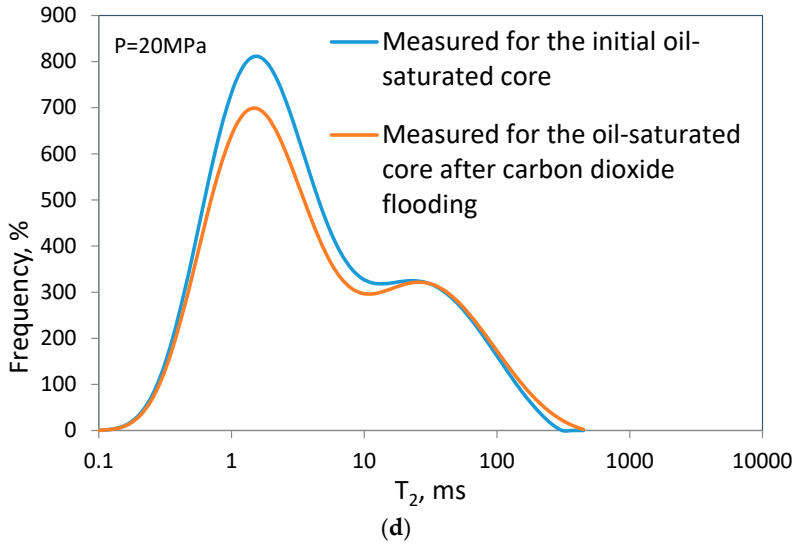

Figure 9. Measured T_2 responses of cores before and after the CO_2 flooding conducted at: (**a**) 8 MPa; (**b**) 13 MPa; (**c**) 16 MPa; and (**d**) 20 MPa.

As depicted in Figure 9a, there is a negligible change in the signal peak area corresponding to the pores within the core when comparing before and after flooding conditions at a pressure of 8 MPa. This suggests that the initial pressure increment has a minimal impact on the core's pore structure. However, as illustrated in Figure 9b, when the pressure elevates to 13 MPa, a significant reduction in the signal from large pores becomes evident. This can be attributed to the dynamics of immiscible flooding, where the oil within large pore throats (10–100 ms) is more readily displaced. In contrast, the substantial capillary forces present in low-permeability cores make the initiation of flow in small pore throats (0.01–10 ms) more challenging. Despite the pressure exceeding the precipitation onset point for asphaltenes, the onset of asphaltene deposition is observed. According to Figure 3c, the initial deposition of asphaltenes tends to occur on the walls of large pores, which are less susceptible to bridging. Consequently, this results in minimal physical damage to the core. Nevertheless, when the pressure surpasses 16 MPa, the scenario shifts during the miscible flooding stage. At this juncture, a substantial influx of CO_2 enters both medium and small pore throats, accelerating the rate of asphaltene deposition within these confined spaces. Under these conditions, asphaltene particles exhibit a robust cohesive force, leading to their aggregation, as shown in Figure 3g. This aggregation can cause significant blockages in pore throats, which correlates with the previously observed changes in gas permeability. The behavior of small pores becomes erratic, potentially due to CO_2's preferential utilization of crude oil within larger and medium-sized pores, as shown in Figure 9c,d. The recovery factor (RF) is predominantly influenced by the contributions from large pores. However, the diffusion of CO_2 into small pores is impeded, and the underlying reaction mechanisms remain unclear. It is hypothesized that this may also be influenced by the deposition and adsorption of asphaltenes within the larger pores, which, upon NMR scanning, may appear as alterations in smaller pores.

4. Conclusions

The damage mechanism of the ultra-low-permeability reservoirs caused by the precipitation and deposition of asphaltene during CO_2 flooding is revealed by experiments.

(1) Utilizing a visual high-pressure tank, the precipitation onset point for asphaltenes was determined. The study revealed that for crude oil from the Changqing X block, this critical threshold is at 12.6 MPa. Notably, this onset point precedes the Minimum Miscibility Pressure (MMP). During the immiscible flooding phase, the extent of asphaltene precipitation escalates with increasing injection pressure. Upon transitioning

to the miscible flooding stage, while asphaltene precipitation continues, it occurs to a significantly lesser degree.

(2) A series of core flooding experiments were performed to assess the impact on recovery factor (RF) and permeability reduction in ultra-low permeability reservoirs. The results indicate that when the pressure is within the interval between the critical deposition pressure and MMP, both RF and the rate of core permeability loss increase with pressure. During the CO_2 miscible flooding process, RF peaks, and the asphaltene content in the produced oil is at its highest, leading to substantial damage to the low-permeability reservoir.

(3) A comparative analysis of the T2 response in oil-saturated cores before and after CO_2 flooding was conducted. It was observed that asphaltene deposition minimally affects core porosity (approximately 8%). This suggests that in instances where the core has high permeability and larger pore-throat dimensions, the asphaltene deposits, which adhere to the pore-throat walls, do not substantially compromise the reservoir's pore space.

Author Contributions: Conceptualization, D.Y. and D.Z.; investigation, Q.L. and D.Z.; data curation, D.Y. and D.Z.; writing—original draft preparation, D.Y.; writing—review and editing, D.Y. and D.Z.; visualization, D.Z.; supervision, D.Z.; funding acquisition, D.Y. and D.Z. All authors have read and agreed to the published version of the manuscript.

Funding: This research was funded by the National Natural Science Foundation of China (NO. 52004247 and NO. 51604243) and Zhoushan Science and Technology Bureau (NO. 2021C21024), China Scholarship Council.

Institutional Review Board Statement: Not applicable.

Informed Consent Statement: Not applicable.

Data Availability Statement: The original contributions presented in the study are included in the article, further inquiries can be directed to the corresponding author.

Acknowledgments: The authors would like to express their appreciation for the School of Petrochemical Engineering & Environment of Zhejiang Ocean University for permission to publish this paper.

Conflicts of Interest: The authors declare no conflicts of interest.

References

1. Rauch, R.; Kiros, Y.; Engvall, K.; Kantarelis, E.; Brito, P.; Nobre, C.; Santos, S.M.; Graefe, P.A. Hydrogen from Waste Gasification. *Hydrogen* **2024**, *5*, 70–101. [CrossRef]
2. Liu, F.; Yue, P.; Wang, Q.; Yu, G.; Zhou, J.; Wang, X.; Fang, Q.; Li, X. Experimental study of oil displacement and gas channeling during CO_2 flooding in ultra—Low permeability oil reservoir. *Energies* **2022**, *15*, 5119. [CrossRef]
3. Bondor, P. Applications of carbon dioxide in enhanced oil recovery. *Energy Convers. Manag.* **1992**, *33*, 579–586. [CrossRef]
4. Gozalpour, F.; Ren, S.R.; Tohidi, B. CO_2 EOR and storage in oil reservoir. *Oil Gas Sci. Technol.* **2005**, *60*, 537–546. [CrossRef]
5. Yu, X.; Chen, H.; Wang, B.; Wang, R.; Shan, Y. Driving forces of CO_2 emissions and mitigation strategies of China's National low carbon pilot industrial parks. *Appl. Energy* **2018**, *212*, 1553–1562. [CrossRef]
6. Zhang, L.; Wang, Y.; Miao, X.; Gan, M.; Li, X. Geochemistry in geologic CO_2 utilization and storage: A brief review. *Adv. Geo-Energy Res.* **2019**, *3*, 304–313. [CrossRef]
7. Ren, J.; Wang, Y.; Feng, D.; Gong, J. CO_2 migration and distribution in multiscale-heterogeneous deep saline aquifers. *Adv. Geo-Energy Res.* **2021**, *5*, 333–346. [CrossRef]
8. Ren, B.; Ren, S.; Zhang, L.; Chen, G.; Zhang, H. Monitoring on CO_2 migration in a tight oil reservoir during CCS-EOR in Jilin Oilfield China. *Energy* **2016**, *98*, 108–121. [CrossRef]
9. Ren, B.; Xu, Y.; Niu, B.; Ren, S.; Li, X.; Guo, P.; Song, X. (Eds.) Laboratory assessment and field pilot of near miscible CO_2 injection for IOR and storage in a tight oil reservoir of Shengli Oilfield China. In Proceedings of the SPE Enhanced Oil Recovery Conference, Kuala Lumpur, Malaysia, 19–21 July 2011; OnePetro: Richardson, TX, USA, 2011.
10. LIU, Z.-F. Key techniques of integrated seismic reservoir characterization for tight oil & gas sands. *Prog. Geophys.* **2014**, *29*, 182–190.
11. Fic, J.; Pedersen, P.K. Reservoir characterization of a "tight" oil reservoir, the middle Jurassic Upper Shaunavon Member in the Whitemud and Eastbrook pools, SW Saskatchewan. *Mar. Pet. Geol.* **2013**, *44*, 41–59. [CrossRef]

12. Shao, X.; Pang, X.; Jiang, F.; Li, L.; Huyan, Y.; Zheng, D. Reservoir characterization of tight sandstones using nuclear magnetic resonance and incremental pressure mercury injection experiments: Implication for tight sand gas reservoir quality. *Energy Fuels* **2017**, *31*, 10420–10431. [CrossRef]
13. Wang, R.; Arkin, K.; Liang, Y.; Li, H.; Zheng, L.; Li, H.; Li, B. Study on Production Characteristics during N2 Flooding in Low Permeability Reservoirs: Effect of Matrix Permeability and Fracture. *Processes* **2023**, *11*, 2112. [CrossRef]
14. Dong, L.; Li, L.; Dong, W.; Wang, M.; Chen, X. Investigation on the Injection Pattern of Intermittent Natural Gas Flooding in Ultra-Low Permeability Reservoirs. *Processes* **2022**, *10*, 2198. [CrossRef]
15. Moradi, S.; Dabiri, M.; Dabir, B.; Rashtchian, D.; Emadi, M. Investigation of asphaltene precipitation in miscible gas injection processes: Experimental study and modeling. *Braz. J. Chem. Eng.* **2012**, *29*, 665–676. [CrossRef]
16. Mousavi, M.; Abdollahi, T.; Pahlavan, F.; Fini, E.H. The influence of asphaltene-resin molecular interactions on the colloidal stability of crude oil. *Fuel* **2016**, *183*, 262–271. [CrossRef]
17. Punase, A.; Prakoso, A.; Hascakir, B. (Eds.) The polarity of crude oil fractions affects the asphaltenes stability. In Proceedings of the SPE Western Regional Meeting, Anchorage, AK, USA, 23–26 May 2016; OnePetro: Richardson, TX, USA, 2016.
18. Gray, M.R.; Tykwinski, R.R.; Stryker, J.M.; Tan, X. Supramolecular Assembly Model for Aggregation of Petroleum Asphaltenes. *Energy Fuels* **2011**, *25*, 3125–3134. [CrossRef]
19. Redelius, P.G. The structure of asphaltenes in bitumen. *Road Mater. Pavement Des.* **2006**, *7*, 143–162. [CrossRef]
20. Guerrero-Martin, C.A.; Montes-Pinzon, D.; Meneses Motta da Silva, M.; Montes-Paez, E.; Guerrero-Martin, L.E.; Salinas-Silva, R.; Camacho-Galindo, S.; Fernandes Lucas, E.; Szklo, A. Asphaltene precipitation/deposition estimation and inhibition through nanotechnology: A comprehensive review. *Energies* **2023**, *16*, 4859. [CrossRef]
21. Jafari Behbahani, T.; Ghotbi, C.; Taghikhani, V.; Shahrabadi, A. (Eds.) Investigation of asphaltene deposition mechanisms during primary depletion and CO_2 injection. In Proceedings of the SPE European Formation Damage Conference, Noordwijk, The Netherlands, 7–9 June 2011; OnePetro: Richardson, TX, USA, 2011.
22. Alta'ee, A.F.; Hun, O.S.; Alian, S.S.; Saaid, I.M. Experimental Investigation on the Effect of CO_2 and WAG Injection on Permeability Reduction Induced by Asphaltene Precipitation in Light Oil. *Ind. Mat. Eng.* **2012**, *6*, 1215–1220.
23. Cao, M.; Gu, Y. Oil recovery mechanisms and asphaltene precipitation phenomenon in immiscible and miscible CO_2 flooding processes. *Fuel* **2013**, *109*, 157–166. [CrossRef]
24. Davudov, D.; Moghanloo, R.G. A new model for permeability impairment due to asphaltene deposition. *Fuel* **2019**, *235*, 239–248. [CrossRef]
25. Cho, J.; Kim, T.H.; Chang, N.; Lee, K.S. Effects of asphaltene deposition-derived formation damage on three-phase hysteretic models for prediction of coupled CO_2 enhanced oil recovery and storage performance. *J. Pet. Sci. Eng.* **2019**, *172*, 988–997. [CrossRef]
26. Leontaritis, K.J.; Amaefule, J.O.; Charles, R.E. A Systematic Approach for the Prevention and Treatment of Formation Damage Caused by Asphaltene Deposition. *SPE Prod. Facil.* **1994**, *9*, 157–164. [CrossRef]
27. Mohammad, R.S.; Zhang, S.; Lu, S.; Jamal-Ud-Din, S.; Zhao, X. Simulation study of asphaltene deposition and solubility of CO_2 in the brine during cyclic CO_2 injection process in unconventional tight reservoirs. *Int. J. Geol. Environ. Eng.* **2017**, *11*, 495–510.
28. Liu, Y.; Fu, M. The Difference in Damage to Low-Permeability Reservoirs by Different Injection Methods of CO_2 Flooding. *Processes* **2023**, *11*, 3260. [CrossRef]
29. Bearsley, S.; Forbes, A.; Haverkamp, R. Direct observation of the asphaltene structure in paving-grade bitumen using confocal laser-scanning microscopy. *J. Microsc.* **2004**, *215*, 149–155. [CrossRef] [PubMed]
30. Srivastava, R.; Huang, S.; Dong, M. Asphaltene deposition during CO_2 flooding. *SPE Prod. Facil.* **1999**, *14*, 235–245. [CrossRef]
31. Wang, C.; Li, T.; Gao, H.; Zhao, J.; Li, H.A. Effect of asphaltene precipitation on CO 2-flooding performance in low-permeability sandstones: A nuclear magnetic resonance study. *RSC Adv.* **2017**, *7*, 38367–38376. [CrossRef]
32. Yuan, B.; Wood, D.A. A comprehensive review of formation damage during enhanced oil recovery. *J. Pet. Sci. Eng.* **2018**, *167*, 287–299. [CrossRef]
33. Soroush, S.; Pourafshary, P.; Vafaie-Sefti, M. (Eds.) A comparison of asphaltene deposition in miscible and immiscible carbon dioxide flooding in porous media. In Proceedings of the SPE EOR Conference at Oil and Gas West Asia, Muscat, Oman, 31 March–2 April 2014; OnePetro: Richardson, TX, USA, 2014.
34. Shen, Z.; Sheng, J.J. Experimental and numerical study of permeability reduction caused by asphaltene precipitation and deposition during CO_2 huff and puff injection in Eagle Ford shale. *Fuel* **2018**, *211*, 432–445. [CrossRef]
35. Moghanloo, R.G.; Davudov, D.; Akita, E. Formation damage by organic deposition. In *Formation Damage During Improved Oil Recovery*; Elsevier: Amsterdam, The Netherlands, 2018.
36. Li, X.; Chi, P.; Guo, X.; Sun, Q. CO_2-induced asphaltene deposition and wettability alteration on a pore interior surface. *Fuel* **2019**, *254*, 115595. [CrossRef]
37. Li, R.; Liao, X.; Zou, J.; Zhang, H.; Zhou, X.; Mu, L.; Dong, P. (Eds.) Experimental and Numerical Studies on Asphaltene Deposition Distribution during CO_2 Flooding in Ultra-Low Permeability Reservoirs. In Proceedings of the Carbon Management Technology Conference, Houston, TX, USA, 15–18 July 2019; OnePetro: Richardson, TX, USA, 2019.
38. Chen, J.; Li, T.; Wu, S. Influence of pressure and CO_2 content on the asphaltene precipitation and oil recovery during CO_2 flooding. *J. Pet. Sci. Eng.* **2018**, *36*, 577–582. [CrossRef]

39. Bouhadda, Y.; Bendedouch, D.; Sheu, E.; Krallafa, A. Some Preliminary Results on a Physico-Chemical Characterization of a Hassi Messaoud Petroleum Asphaltene. *Energy Fuels* **2000**, *14*, 845–853. [CrossRef]
40. ASTM. Standard test method for characteristic groups in rubber extender and processing oils and other petroleum-derived oils by the clay-gel absorption chromatographic method. In *Annual Book of ASTM Standards*; Philadelphia, Sec.; ASTM: West Conshohocken, PA, USA, 2007; Volume 5.
41. Song, Z.; Zhu, W.; Wang, X.; Guo, S. 2-D pore-scale experimental investigations of asphaltene deposition and heavy oil recovery by CO_2 flooding. *Energy Fuels* **2018**, *32*, 3194–3201. [CrossRef]
42. Zanganeh, P.; Dashti, H.; Ayatollahi, S. Visual investigation and modeling of asphaltene precipitation and deposition during CO_2 miscible injection into oil reservoirs. *Fuel* **2015**, *160*, 132–139. [CrossRef]
43. Fakher, S.; Imqam, A. Asphaltene precipitation and deposition during CO_2 injection in nano shale pore structure and its impact on oil recovery. *Fuel* **2019**, *237*, 1029–1039. [CrossRef]
44. Zanganeh, P.; Ayatollahi, S.; Alamdari, A.; Zolghadr, A.; Dashti, H.; Kord, S. Asphaltene deposition during CO_2 injection and pressure depletion: A visual study. *Energy Fuels* **2012**, *26*, 1412–1419. [CrossRef]
45. Wang, Z.; Yang, S.; Lei, H.; Yang, M.; Li, L.; Yang, S. Oil recovery performance and permeability reduction mechanisms in miscible CO_2 water-alternative-gas (WAG) injection after continuous CO_2 injection: An experimental investigation and modeling approach. *J. Pet. Sci. Eng.* **2017**, *150*, 376–385. [CrossRef]
46. Jafari Behbahani, T.; Ghotbi, C.; Taghikhani, V.; Shahrabadi, A. Investigation on asphaltene deposition mechanisms during CO_2 flooding processes in porous media: A novel experimental study and a modified model based on multilayer theory for asphaltene adsorption. *Energy Fuels* **2012**, *26*, 5080–5091. [CrossRef]